Pressure-induced novel compounds in the Hf-O system from first-principles calculations

Jin Zhang,[1,*] Artem R. Oganov,[2,1,3,4,†] Xinfeng Li,[5] Kan-Hao Xue,[6] Zhenhai Wang,[7] and Huafeng Dong[8]

[1]*Department of Geosciences, Center for Materials by Design, and Institute for Advanced Computational Science, State University of New York, Stony Brook, New York 11794-2100, USA*

[2]*Skolkovo Institute of Science and Technology, Skolkovo Innovation Center, 5 Nobel Street, Moscow 143026, Russia*

[3]*Science and Technology on Thermostructural Composite Materials Laboratory, International Center for Materials Discovery, School of Materials Science and Engineering, Northwestern Polytechnical University, Xi'an, Shaanxi 710072, People's Republic of China*

[4]*Moscow Institute of Physics and Technology, Dolgoprudny, Moscow Region 141700, Russia*

[5]*State Key Laboratory for Mechanical Behavior of Materials, School of Materials Science and Engineering, Xi'an Jiaotong University, Xi'an, 710049, People's Republic of China*

[6]*School of Optical and Electronic Information, Huazhong University of Science and Technology, Wuhan 430074, China*

[7]*Peter Grünberg Research Center, Nanjing University of Posts and Telecommunications, Nanjing, Jiangsu 210003, China*

[8]*School of Physics and Optoelectronic Engineering, Guangdong University of Technology, Guangzhou 510006, China*

(Received 9 August 2015; revised manuscript received 7 October 2015; published 13 November 2015)

Using first-principles evolutionary simulations, we have systematically investigated phase stability in the Hf-O system at pressure up to 120 GPa. New compounds Hf_5O_2, Hf_3O_2, HfO, and HfO_3 are discovered to be thermodynamically stable at certain pressure ranges. Two new high-pressure phases are found for Hf_2O: one with space group *Pnnm* and anti-$CaCl_2$-type structure, another with space group $I4_1/amd$. *Pnnm*-HfO_3 shows interesting structure, simultaneously containing oxide O^{2-} and peroxide $[O\text{-}O]^{2-}$ anions. Remarkably, it is $P\bar{6}2m$-HfO rather than OII-HfO_2 that exhibits the highest mechanical characteristics among Hf-O compounds. *Pnnm*-Hf_2O, *Imm*2-Hf_5O_2, $P\bar{3}1m$-Hf_2O, and $P\bar{4}m2$-Hf_2O_3 phases also show superior mechanical properties; theoretically these phases become metastable phases to ambient pressure and their properties can be exploited.

DOI: 10.1103/PhysRevB.92.184104 PACS number(s): 61.50.Ks, 62.20.Qp, 64.30.Jk

I. INTRODUCTION

Hafnium oxide HfO_2 has a wide range of technological applications. In the electronics industry, hafnium oxide-based material is currently used as an excellent high-k gate dielectric [1] and oxygen-deficient hafnium oxide has also received additional interest for resistive-switching memories [2]. As for other applications, even though the hardness of hafnia (HfO_2) is not that high for it to be considered as a superhard material [3], it still attracts attention as a potential candidate for hard oxide-based materials [4]. Unlike carbides or nitrides, oxides are more stable in the oxygen atmosphere at high temperature, which is valuable for many applications. Many oxide ceramics, especially those involving transition metals, are promising for application as hard coatings, since metal d electrons and strong bonds define their remarkable mechanical properties (high hardness, good chemical resistance, high tensile strength, and good fracture toughness) [5]. As compared to most transition-metal oxide ceramics, hafnium oxide ceramics exhibit enhanced mechanical properties (higher fracture toughness) and structural stability (low thermal conductivity). Here, we want to explore all possible stable compounds of the Hf-O system at pressures up to 120 GPa.

Under ambient temperature, experiments [6,7] indicated that pure Hf is stable in the α phase (hexagonal-close-packed structure, space group: $P6_3/mmc$) and transforms to ω phase (hexagonal structure, space group: $P6/mmm$) at 46–58 GPa and then to β-Hf (body-centered cubic, space group: $Im\bar{3}m$) at 71.1–78.4 GPa. Our generalized gradient approximation (GGA) calculated results indicate the transition pressures: α phase $\rightarrow$ ω phase at 49 GPa and ω phase $\rightarrow$ β-Hf at 70 GPa, which are in accord with the above experimental results. It has been suggested that the solubility of oxygen in the octahedral interstitial sites of α-Hf (hcp-Hf) can be as high as 20 at.% [8], while solubility of oxygen in β-Hf (bcc-Hf) is only 3 at.% [9]. Several experimental [10,11] and theoretical studies [12,13] have investigated the interstitial oxygen in hcp-Hf. Now it is well established that three stoichiometric compositions, Hf_6O, Hf_3O, and Hf_2O, can be formed with increasing occupation of the octahedral-interstitial positions in hcp-Hf by oxygen atoms. Hf_2O_3 was theoretically predicted to form upon increasing the concentration of oxygen vacancies in monoclinic HfO_2 [14].

The phase sequence of HfO_2 at ambient temperature with increasing pressure is baddeleyite (monoclinic, space group: $P2_1/c$) $\rightarrow$ orthorhombic I (orthorhombic, space group: *Pbca*, OI) $\rightarrow$ orthorhombic II (orthorhombic, space group: *Pnma*, OII) [15–17]. Orthorhombic OII-HfO_2 with experimentally reported hardness between 6 and 13 GPa [18] has been speculated to be much harder than the low-pressure phases (baddeleyite and OI-HfO_2) because of its comparatively high bulk modulus [5,19].

In this study, we systematically investigate the structure and stability of Hf-O compounds up to a pressure of 120 GPa by the first-principles evolutionary algorithm USPEX. Several new stoichiometries in the Hf-O system have been predicted under high pressure. Furthermore, we verify the dynamical and mechanical stability of these new high-pressure phases at 0 GPa by calculating their phonons and elastic constants. To better understand the correlations between hardness and O content, we estimate the hardness of these phases at 0 GPa using Chen's hardness model [20]. Quenchable high-pressure

*Corresponding author: jin.zhang.1@stonybrook.edu

†Corresponding author: artem.oganov@stonybrook.edu

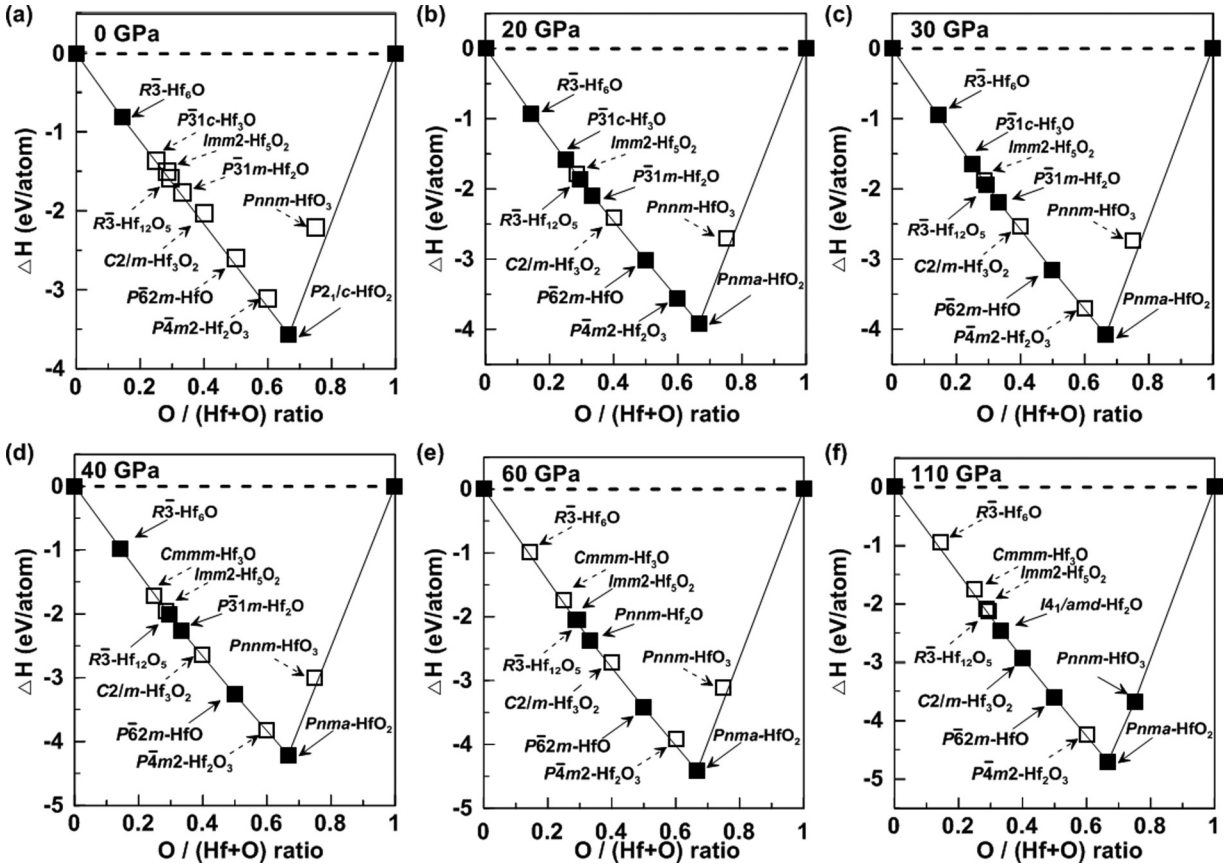

FIG. 1. Convex hull diagrams for the Hf-O system at (a) 0 GPa, (b) 20 GPa, (c) 30 GPa, (d) 40 GPa, (e) 60 GPa, and (f) 110 GPa, respectively. Solid squares and solid-line arrows denote stable phases while open squares and dashed-line arrows represent the compounds for comparison.

phases often possess superior mechanically properties, and we indeed find novel hafnium oxides with unusual mechanical properties.

II. COMPUTATIONAL METHODOLOGY

Searching the stable high-pressure structures in the Hf-O system was done using the first-principles evolutionary algorithm (EA) as implemented in the USPEX code [21–23] combined with *ab initio* structure relaxations using density functional theory (DFT) with the Perdew-Burke-Ernzerhof (PBE)–GGA functional [24], as implemented in the VASP package [25]. In our work, variable-composition structure searches [23] for the Hf-O system with up to 32 atoms in the unit cell were performed at 0, 10, 20, 30, 40, 50, 60, 70, 80, 90, 100, 110, and 120 GPa. The initial generation of structures was produced randomly using space-group symmetry; each subsequent generation was obtained by variation operators including heredity (40%), lattice mutation (20%), random (20%), and transmutation (20%). The electron-ion interaction was described by the projector-augmented wave (PAW) pseudopotentials [26], with $5p^6 6s^2 5d^4$ and $2s^2 2p^4$ shells treated as valence for Hf and O, respectively. The generalized gradient approximation (GGA) in the Perdew-Burke-Ernzerhof form [24] was utilized for describing exchange-correlation effects. The plane-wave energy cutoff was chosen as 600 eV and Γ-centered uniform k meshes with resolution $2\pi \times 0.06$ Å^{-1} were used to sample the Brillouin zone, resulting in excellent convergence. Phonon dispersions were calculated using the finite-displacement method with the Phonopy code [27].

III. RESULTS AND DISCUSSIONS

A. Crystal structure prediction for the Hf-O system

Thermodynamic convex hull, which defines stable compounds, is based on the free enthalpies (at $T = 0$ K, enthalpies) of the compounds and pure elements in their stable forms. The high-pressure convex hull and pressure-composition phase diagram of the Hf-O system are depicted in Figs. 1 and 2, respectively. See Supplemental Material Fig. S1 [28] for detailed convex hull information of Hf-O compounds at a certain pressure. Besides the three well-known phases of HfO_2 and three suboxides ($R\bar{3}$-Hf_6O, $R\bar{3}c$-Hf_3O, and $P\bar{3}1m$-Hf_2O), our structure searches found hitherto unknown compounds with new stoichiometries, including Hf_5O_2, Hf_3O_2, HfO, and HfO_3. Note that two new high-pressure phases of Hf_2O (denoted as *Pnnm*-Hf_2O and $I4_1/amd$-Hf_2O) were also found by our searches. Recent work [29] indicated that $Hf_{12}O_5$ is a stable compound at low temperature, disproportionate above 220 K, therefore it is not expected to be observed experimentally. Our work indicates that $Hf_{12}O_5$ is actually stable only in the pressure range 8–37 GPa. The related thermodynamic stability, dynamical stability, mechanical stability, phase status at 0 GPa,

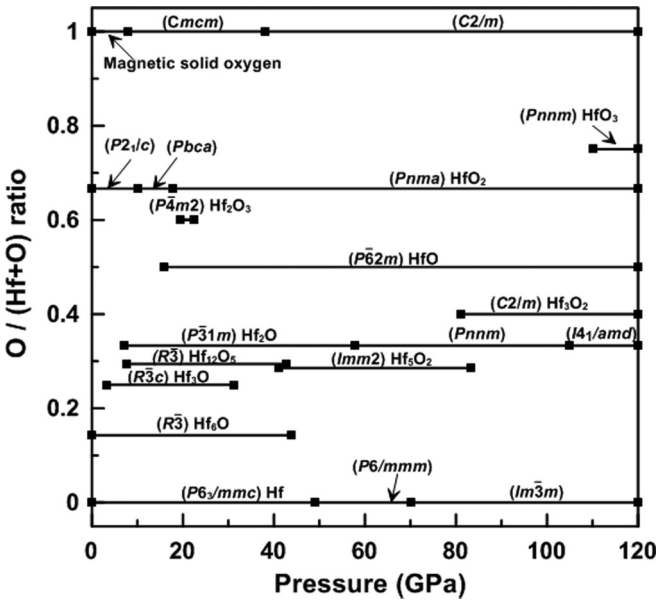

FIG. 2. Pressure-composition phase diagram of the Hf-O system.

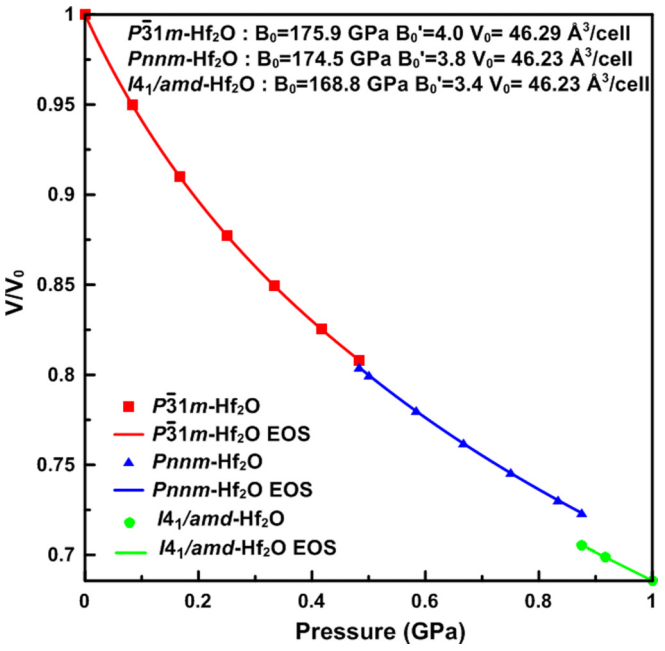

FIG. 3. (Color online) Equation of state of Hf_2O. Our calculations were fit to a third-order Birch-Murnaghan equation of state to find B_0 and B_0'.

and calculated stable pressure ranges for Hf-O compounds are listed in Table I.

Our calculation confirms that Hf_2O_3 proposed by Xue [14] can exist as a metastable phase (it is dynamically and mechanically stable at 0 GPa), and shows that it should be a stable phase in the pressure range 20–23 GPa. The predicted transition from monoclinic-HfO_2 to OI-HfO_2 occurs at 10 GPa, which coincides with experimental observations [15]. The transition from OI-HfO_2 to OII-HfO_2 occurs at 18 GPa, which is lower than the experimental result 30–37 GPa [3,15] but in good agreement with other theoretical estimates of 17 GPa [3]. Furthermore, our calculated result shows that OII-HfO_2 is stable up to at least 120 GPa, which agrees with previous experimental work [3]. According to our predictions, only baddeleyite-type HfO_2 and $R\bar{3}$-Hf_6O are stable at 0 GPa, in contrast with the Zr-O system (Zr_6O, Zr_3O, Zr_2O, ZrO, and ZrO_2 are stable at 0 GPa) [30].

In order to study the ordering of interstitial oxygen atoms in hcp-HfO_x, Hirabayashi *et al.* [10] used electron, neutron, and x-ray diffraction to analyze single crystals containing 13.4 at.% O and 15.8 at.% O and found two types of interstitial superstructures: $HfO_{1/6-}$ and $HfO_{1/6+}$ below 600 K. The space group of $HfO_{1/6-}$ reported by Hirabayashi [10] is $R\bar{3}$, which

TABLE I. Thermodynamic stability (TS), dynamical stability (DS), mechanical stability (MS), phase status (PS) at 0 GPa and calculated pressure ranges of stability for Hf-O compounds. Thermodynamic stability means that this structure is located on the convex hull at 0 GPa; dynamical stability means that no imaginary frequency exits in the whole Brillouin zone in the phonon dispersion curves at 0 GPa; mechanical stability means that the elastic constants matrix is positive definite at 0 GPa. $\surd$ = thermodynamic or dynamical or mechanical stability; $\times$ = thermodynamic or dynamical or mechanical instability.

Compound	Space group	TS	DS	MS	PS	Stable pressure This work	Range (GPa) Ref. [3]
Hf_6O	$R\bar{3}$	$\surd$	$\surd$	$\surd$	stable	0–43.9	
Hf_3O	$R\bar{3}c$	$\times$	$\surd$	$\surd$	metastable	3.3–31.3	
Hf_5O_2	$Imm2$	$\times$	$\surd$	$\surd$	metastable	41–83.3	
$Hf_{12}O_5$	$R\bar{3}$	$\times$	$\surd$	$\surd$	metastable	7.7–42.8	
Hf_2O	$P\bar{3}1m$	$\times$	$\surd$	$\surd$	metastable	7.2–57.7	
Hf_2O	$Pnnm$	$\times$	$\surd$	$\surd$	metastable	57.7–105	
Hf_2O	$I4_1/amd$	$\times$	$\times$	$\surd$	unstable	105–120	
Hf_3O_2	$C2/m$	$\times$	$\surd$	$\surd$	metastable	81.1–120	
HfO	$P\bar{6}2m$	$\times$	$\surd$	$\surd$	metastable	16–120	
Hf_2O_3	$P\bar{4}m2$	$\times$	$\surd$	$\surd$	metastable	19.5–22.5	
HfO_2	$P2_1/c$	$\surd$	$\surd$	$\surd$	stable	0–10	0–9.1
HfO_2	$Pbca$	$\times$	$\surd$	$\surd$	metastable	10–17.9	9.1–16.8
HfO_2	$Pnma$	$\times$	$\surd$	$\surd$	metastable	17.9–120	16.8–
HfO_3	$Pnnm$	$\times$	$\times$	$\surd$	unstable	110–120	

TABLE II. Structural parameters of *Imm*2-Hf_5O_2, *Pnnm*-Hf_2O, *C*2/*m*-Hf_3O_2, $P\bar{6}2m$-HfO, *C*2/*m*-Hf_2O_3, and *Pnnm*-HfO_3 at 0 GPa.

Compound	Space group	Enthalpy of formation (eV/atom)	Lattice constants (Å)	Wyckoff positions	*x*	*y*	*z*
Hf_5O_2	*Imm*2	−1.52	$a = 14.455$	Hf 4*c*	0.711	0.50	0.566
			$b = 3.141$	Hf 2*b*	0.00	0.50	0.098
			$c = 5.082$	Hf 4*c*	0.097	0.00	0.594
				O 4*c*	0.645	0.00	0.818
Hf_2O	*Pnnm*	−1.76	$a = 5.092$	Hf 4*g*	0.263	0.341	0.50
			$b = 5.723$	O 2*c*	0.00	0.50	0.00
			$c = 3.175$				
Hf_2O	$I4_1/amd$	−1.67	$a = 4.554$	Hf 8*e*	1.00	0.50	0.50
			$c = 8.920$	O 4*b*	1.00	1.00	0.50
Hf_3O_2	*C*2/*m*	−2.04	$a = 11.967$	Hf 4*i*	0.625	0.50	0.007
			$b = 3.131$	Hf 4*i*	0.465	0.00	0.346
			$c = 11.198$	Hf 4*i*	0.286	0.00	0.676
			$\beta = 99.67^\circ$	O 4*i*	0.378	0.50	0.607
				O 4*i*	0.787	0.00	0.192
HfO	$P\bar{6}2m$	−2.60	$a = 5.230$	Hf 1*b*	0.00	0.00	0.50
			$c = 3.187$	Hf 2*c*	0.667	0.333	0.00
				O 3*g*	0.00	0.592	0.50
Hf_2O_3	$P\bar{4}m2$	−3.11	$a = 3.137$	Hf 2*g*	0.00	0.50	0.744
			$c = 5.638$	O 2*g*	0.00	0.50	0.135
				O 1*c*	0.50	0.50	0.50
HfO_3	*Pnnm*	−2.22	$a = 6.027$	Hf 4*g*	0.801	0.693	0.00
			$b = 6.172$	O 4*g*	0.067	0.399	0.50
			$c = 3.958$	O 4*g*	0.340	0.141	0.50
				O 4*e*	0.50	0.50	0.312

is identical to our findings. The space group of $HfO_{1/6+}$ is $P\bar{3}1c$ in Hirabayashi's experiment [10]. At 0 K and 0 GPa, our results produce three energetically competitive phases for Hf_3O and their ordering by energy is $R\bar{3}c$-Hf_3O (−10.075 eV/atom) < $P\bar{3}1c$-Hf_3O (−10.072 eV/atom) < $P6_322$-Hf_3O

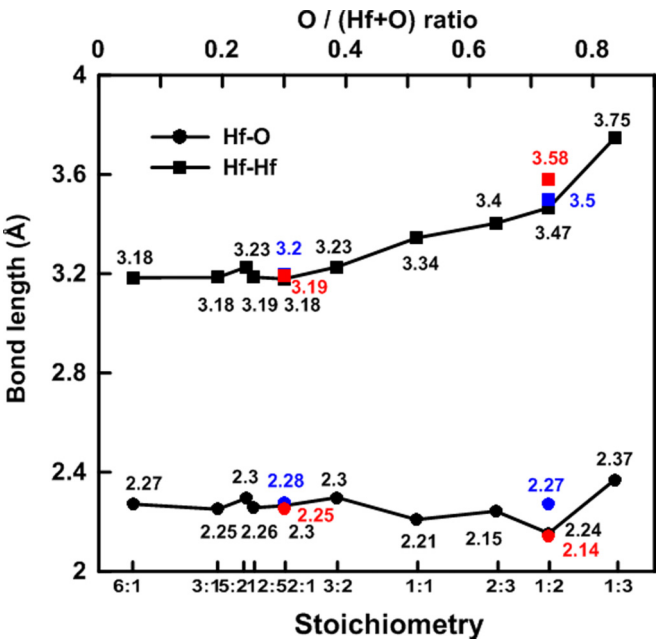

FIG. 4. (Color online) Average bond lengths in Hf-O compounds at 0 GPa.

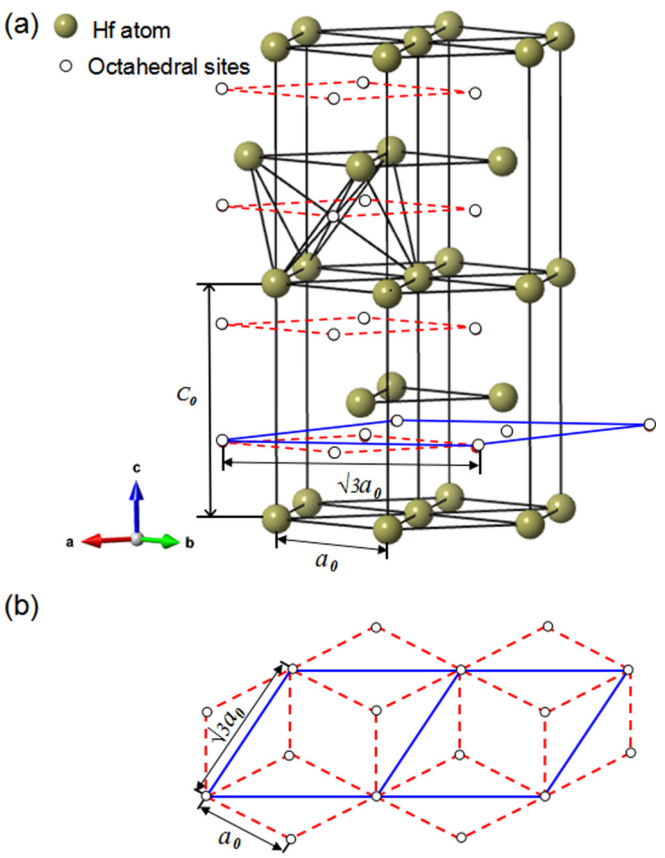

FIG. 5. (Color online) Octahedral voids in hcp hafnium.

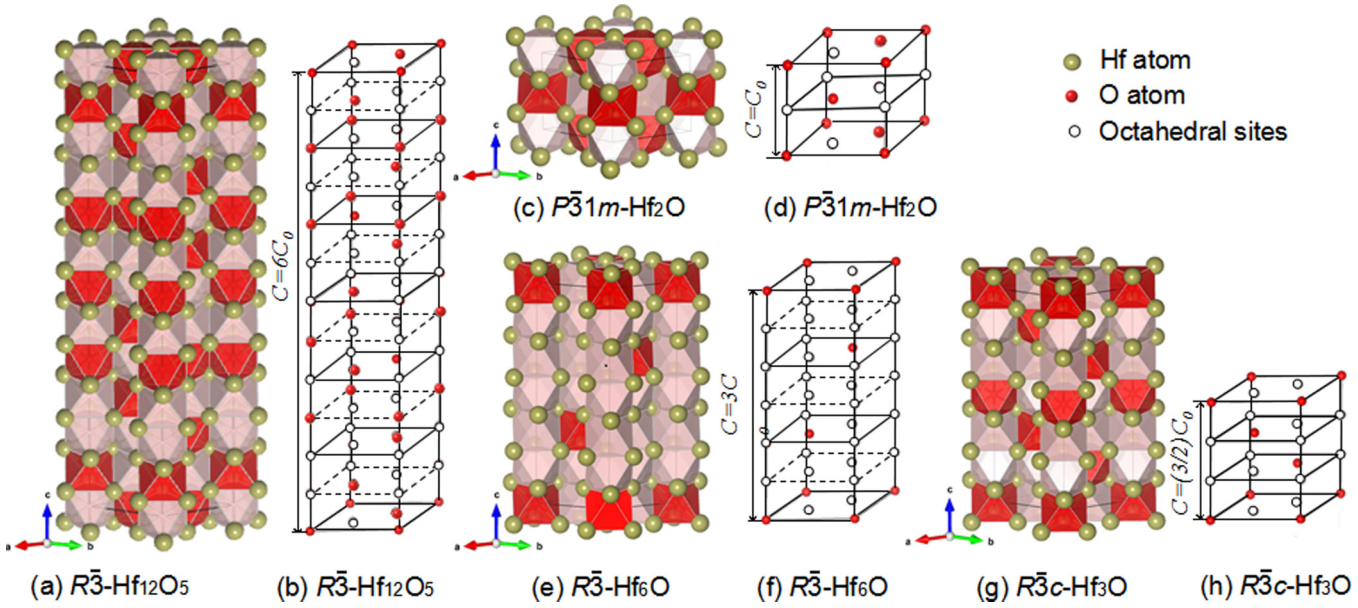

FIG. 6. (Color online) Oxygen sublattice representation (arrangement of oxygen atoms in the octahedral interstitial sites) and polyhedral representation of (a) and (b) $R\bar{3}$-$Hf_{12}O_5$, (c) and (d) $P\bar{3}1m$-Hf_2O, (e) and (f) $R\bar{3}$-Hf_6O, (g) and (h) $R\bar{3}c$-Hf_3O. Oxygen-centered octahedra and oxygen vacancies are shown in red and pink polyhedra, respectively. Oxygen sublattice representations (b), (d), (f), and (h) show only oxygen atoms (filled circles) and vacancies (open circles).

(−10.069 eV/atom). Therefore, one can note that $P\bar{3}1c$-Hf_3O ($P\bar{3}1c$-Zr_3O type), exhibits very close but higher energy than $R\bar{3}c$-Hf_3O at 0 GPa and 0 K. In order to consider the effects of temperature, the quasiharmonic free energy of $R\bar{3}c$-Hf_3O and $P\bar{3}1c$-Hf_3O were calculated using the Phonopy code [27]. The results indicate that free energy of $P\bar{3}1c$-Hf_3O decreases faster than that of $R\bar{3}c$-Hf_3O with temperature, enabling $P\bar{3}1c$-Hf_3O to become more stable than $R\bar{3}c$-Hf_3O at 1000 K, thus explaining the experimental result.

Hf_2O undergoes a trigonal-to-orthorhombic I phase transition 58 GPa and orthorhombic I-to-orthorhombic II transition at 105 GPa. The crystal structure of the new high-pressure phase $Pnnm$-Hf_2O is anti-$CaCl_2$-type. The Birch-Murnaghan equation of state (EOS) [31] was used to fit the compressional behavior of the predicted Hf_2O phases (Fig. 3). The third-order Birch-Murnaghan EOS is given as (1). Most materials have $3 \leqslant B_0' \leqslant 6$ [32,33]. The B_0' of $P\bar{3}1m$-Hf_2O, $Pnnm$-Hf_2O, and $I4_1/amd$-Hf_2O is 4.0, 3.8, and 3.4,

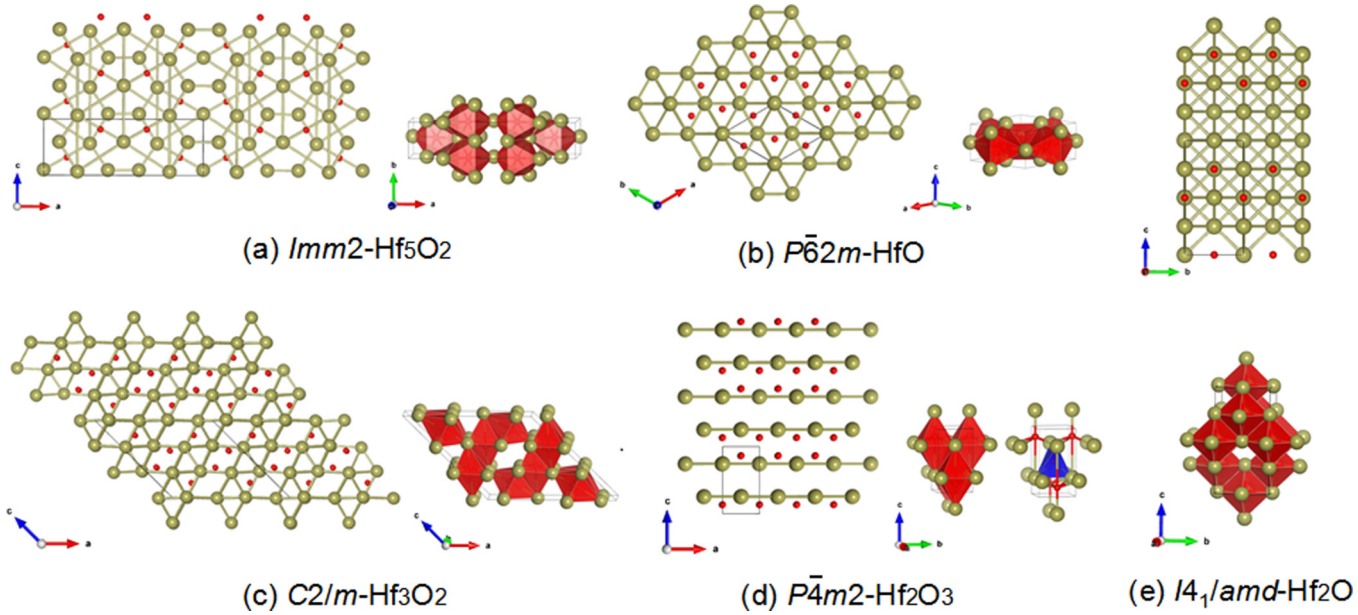

FIG. 7. (Color online) Crystal structures of (a) $Imm2$-Hf_5O_2, (b) $P\bar{6}2m$-HfO, (c) $P\bar{4}m2$-Hf_2O_3, (d) $P\bar{4}m2$-Hf_2O_3, and (e) $I4_1/amd$-Hf_2O. O-centered octahedra and O-centered tetrahedra are shown in red and blue polyhedra, respectively. Large spheres: Hf atoms; small spheres: O atoms.

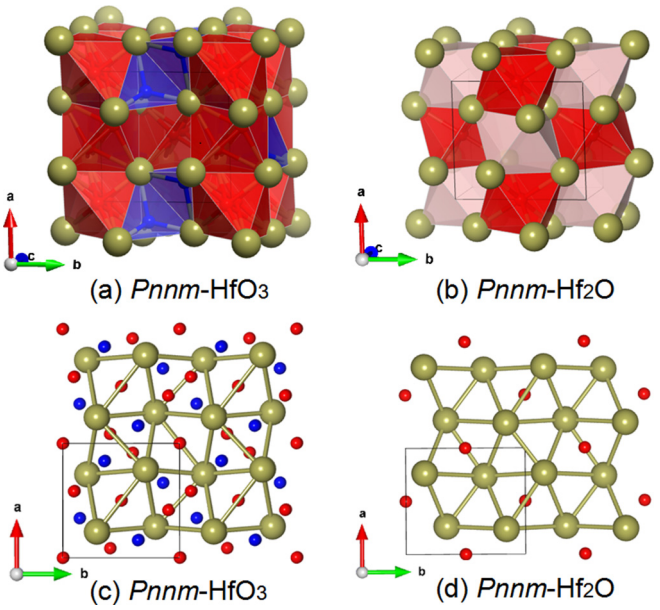

FIG. 8. (Color online) Crystal structure of (a) *Pnnm*-HfO_3, (b) *Pnnm*-Hf_2O, (c) *Pnnm*-HfO_3, (d) *Pnnm*-Hf_2O.

respectively,

$$P(V) = \frac{3B_0}{2}\left[\left(\frac{V}{V_0}\right)^{-7/3} - \left(\frac{V}{V_0}\right)^{-5/3}\right] \times \left\{1 + \frac{3}{4}(B_0' - 4)\left[\left(\frac{V}{V_0}\right)^{-2/3} - 1\right]\right\}. \quad (1)$$

B. Structures of the Hf-O compounds

Table II lists the detailed crystallographic data of *Imm*2- Hf_5O_2, *Pnnm*- Hf_2O, $I4_1/amd$-Hf_2O, $C2/m$-Hf_3O_2, $P\bar{6}2m$-HfO, $C2/m$-Hf_2O_3, and *Pnnm*-HfO_3 compounds at 0 GPa. The mechanical stabilities of all the Hf-O compounds have been checked by the mechanical stability restrictions [34] at 0 GPa; see the Supplemental Material [28] for the criteria of mechanical stability. Except the three well-known structures: baddeleyite-HfO_2, orthorhombic I-HfO_2, II-HfO_2, the dynamical stabilities of all the other phases are checked by calculating phonon dispersion (see Supplemental Material Fig. S2 [28] for detail). Except for *Pnnm*-HfO_3 and $I4_1/amd$-Hf_2O, no imaginary phonon frequencies are found in the whole Brillouin zone at both ambient and high pressure, which means that they are dynamically stable and probably quenchable to ambient pressure. In contrast, HfO_3 and $I4_1/amd$-Hf_2O are stable only at high pressure, but at 0 GPa show total dynamical instability and most likely decomposes. The special electronic structure of HfO_3 will be discussed below. The weighted average lengths of Hf-Hf and Hf-O bonds in Hf-O compounds are plotted in Fig. 4.

Structurally, hafnium oxides can be divided into four groups: suboxides with oxygen interstitials in hcp-Hf (Hf_6O, Hf_3O, $Hf_{12}O_5$, and $P\bar{3}1m$-Hf_2O); other suboxides (Hf_5O_2, *Pnnm*-Hf_2O, $I4_1/amd$-Hf_2O, and HfO); normal oxides (Hf_2O_3, HfO_2); and oxide peroxide (HfO_3). The octahedral sites of hcp hafnium metal are depicted in Fig. 5. Oxygen atoms prefer to occupy these octahedral sites and form ordered structures $R\bar{3}$-Hf_6O, $R\bar{3}c$-Hf_3O, $R\bar{3}$-$Hf_{12}O_5$, and $P\bar{3}1m$-Hf_2O, as shown in Figs. 6(a)–6(d), where Hf atom sites are omitted. The polyhedral representation of these structures is shown in Figs. 5(e)–5(h). Anti-$CaCl_2$-type (*Pnnm*) structure of Hf_2O can also be represented as an hcp sublattice (distorted) of Hf atoms, where half of the octahedral voids are occupied by O atoms. The structure of Hf_3O_2 can be considered to be defective because each layer lacks some Hf atoms to form a Hf-graphene layer. These vacancies are responsible for low values of the mechanical properties of Hf_3O_2.

Similar to ZrO, the structure of HfO contains Hf-graphene layers stacked on top of each other (Zr-Zr distances within the layer are 3.01 Å, and between the layers 3.18 Å), as illustrated in Fig. 7(b), as well as additional Hf and O atoms. The structure can be represented as the ω phase of Hf, intercalated with

TABLE III. Calculated bulk modulus B, shear modulus G, Young's modulus E, Poisson's ratio υ, and hardness of Hf-O compounds, compared with literature data for HfO_2 at 0 GPa. All properties are in GPa (except dimensionless G/B and υ).

Compound		Space group	P	B_H	G_H	E	G/B	υ	H_υ
Hf_6O	this work	$R\bar{3}$	0	129.2	72.8	183.8	0.56	0.26	9.55
Hf_3O	this work	$R\bar{3}c$	0	150.3	78.8	201.3	0.52	0.28	9.1
Hf_5O_2	this work	*Imm*2	0	150.0	95.3	235.9	0.64	0.24	13.9
$Hf_{12}O_5$	this work	$R\bar{3}$	0	163.3	94.5	237.7	0.58	0.26	12.1
Hf_2O	this work	$P\bar{3}1m$	0	175.2	103.1	258.6	0.59	0.25	13.2
Hf_2O	this work	*Pnnm*	0	173.0	110.3	272.9	0.64	0.23	15.5
Hf_2O	this work	$I4_1/amd$	0	159.1	65.1	171.9	0.41	0.32	5.1
Hf_3O_2	this work	$C2/m$	0	154.2	75.9	195.6	0.49	0.29	8.0
HfO	this work	$P\bar{6}2m$	0	210.7	128.1	319.5	0.61	0.25	16.1
Hf_2O_3	this work	$P\bar{4}m2$	0	243.9	127.1	324.8	0.52	0.28	12.9
HfO_2	this work	$P2_1/c$	0	203.6	99.2	256.1	0.49	0.29	9.7
	experiment [41]		0						9.9
HfO_2	this work	*Pbca*	0	225.9	115.8	296.6	0.51	0.28	11.7
HfO_2	this work	*Pnma*	0	226.3	93.8	247.3	0.41	0.31	7.2
	experiment [37]		0						6–13
HfO_3	this work	*Pnnm*	0	171.1	73.6	193.0	0.43	0.31	6.2

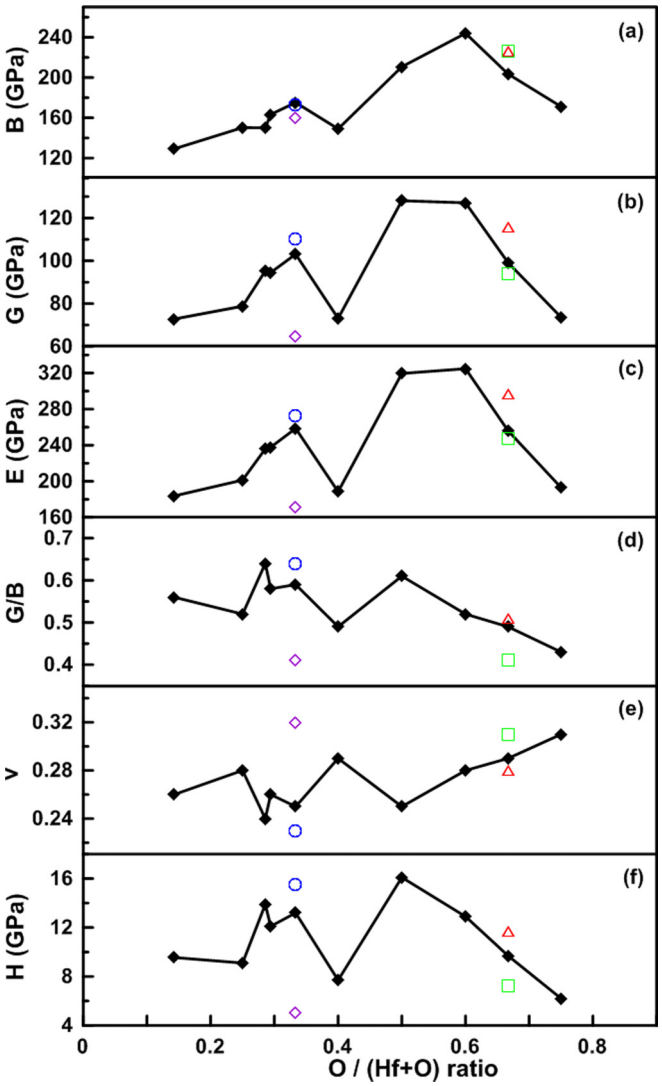

FIG. 9. (Color online) Compositional dependence of the computed mechanical properties of Hf-O compounds. The blue open circle represents *Pnnm*-Hf_2O; purple open diamond represents $I4_1/amd$-Hf_2O; red open triangle represents OI-HfO_2; green open square represents OII-HfO_2.

oxygen atoms. This structure, therefore, is built by a three-dimensional (3D) framework of short and strong Hf-O bonds, reinforced by rather strong Hf-Hf bonds. The former lead to high hardness, the latter improve toughness. $P\bar{4}m2$-Hf_2O_3, which was first proposed by Xue [14], has eightfold and sixfold coordination of Hf atoms, as shown in Fig. 7.

Pnnm-HfO_3 becomes stable at pressures above to 110 GPa. This high-pressure phase originally derives from the oxygen atom dissolving in both octahedral and tetrahedral voids of a heavily distorted hcp-Hf, as shown in Fig. 8(a). However, due to short distances between tetrahedral voids in the hcp structures, some O atoms form pairs and as a result HfO_3 simultaneously contains oxide O^{2-} and peroxide $[O\text{-}O]^{2-}$ anions, and can be described as "oxide peroxide." The O-O bond length in HfO_3 is 1.44 Å at 110 GPa, which is a little smaller than the O-O bond length in peroxide $[O\text{-}O]^{2-}$ ion with 1.47 Å [35] at ambient conditions. It seems that peroxides and oxide peroxides (e.g., Al_4O_7 and AlO_2) become stabilized in many systems under pressure [36].

C. Mechanical properties of Hf-O compounds

Previous studies [15,19,37] suggested that the dense high-pressure phase OII-HfO_2 is quenchable to ambient conditions and has a high bulk modulus, and might be superhard ($H > 40$ GPa). However a recent study [3] reported that the hardness of OII-HfO_2 is well below 40 GPa and therefore this phase is not superhard. Interestingly, our systematic results not only confirm the known hardness of HfO_2 polymorphs: $H(\text{OII}) < H(\text{MI}) < H(\text{OI})$, but also suggest that HfO has the highest hardness among all hafnium oxides; see Fig. 10(f). In addition, *Pnnm*-Hf_2O and *Imm*2-Hf_5O_2 also exhibit higher hardness than other Hf-O compounds, as shown in Table III. The hardness of Hf-O compounds does not monotonically change with O content, but a maximum at HfO.

The calculated modulus B, shear modulus G, Young's modulus E, Poisson's ratio υ, and the hardness of all stable Hf-O compounds are depicted in Table II and Fig. 10 (for comparison, the elastic data of the high-pressure phase $I4_1/amd$-Hf_2O and *Pnnm*-HfO_3 are reported at 0 GPa although they are unstable at 0 GPa). The determination of the bulk modulus B and shear modulus G of polycrystalline aggregates from individual elastic constants c_{ij} can be established from the continuum theories based on Reuss [38] and Voigt [39] approaches that effective isotropic elastic constants are obtained by averaging the anisotropic elastic constants over all possible orientations of the grains in a polycrystal. B_R, B_V and G_R, G_V are respectively the bulk modulus and shear modulus from the Reuss and Voigt approximations (see equations from the supplemental Material [28]). Hill [40] proved that the Voigt and Reuss moduli are upper and lower bounds, and the actual elastic moduli for polycrystals can be approximated by the arithmetic mean of these two extremes. We have therefore utilized the Voigt-Reuss-Hill (VRH) approximation and expressed it as follows:

$$B_{\text{VRH}} = \tfrac{1}{2}(B_V + B_R), \tag{2}$$

$$G_{\text{VRH}} = \tfrac{1}{2}(G_V + G_R). \tag{3}$$

Using the calculated values for B and Young's modulus E and Possion's ratio can be further calculated using the following relationships:

$$E = \frac{9BG}{3B + G}, \tag{4}$$

$$\nu = \frac{3B - 2G}{2(3B + G)}. \tag{5}$$

From Fig. 9 we can conclude that the high O content in the crystal does not guarantee high hardness of Hf-O compounds and the structure plays an important role in determining mechanical properties as we discussed above. The Vickers hardness was calculated according to Chen's model [20]. The corresponding expression is given as follows:

$$H_v = 2(k^2G)^{0.585} - 3, \tag{6}$$

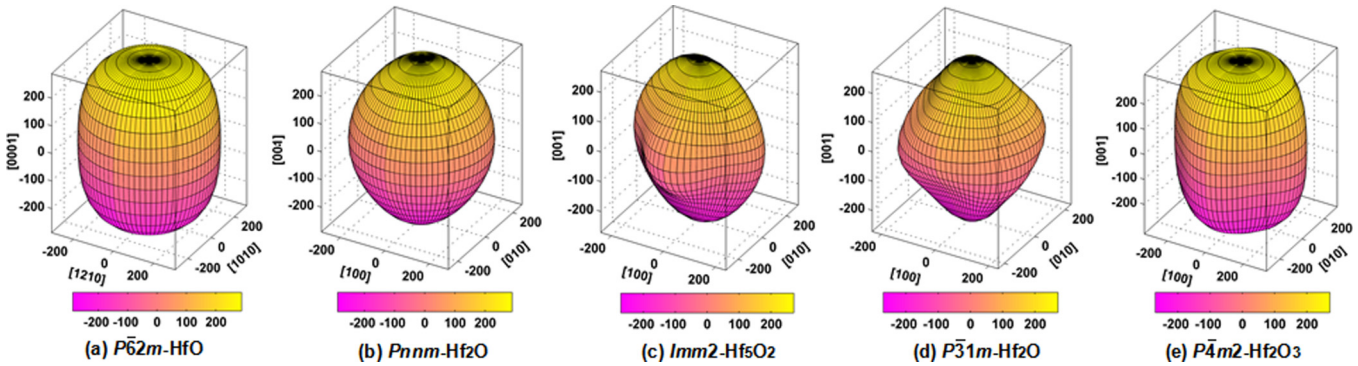

FIG. 10. (Color online) Orientational dependence of Young's moduli (in GPa) of (a) $P\bar{6}2m$-HfO, (b) $Pnnm$-Hf_2O, (c) $Imm2$-Hf_5O_2, (d) $P\bar{3}1m$-Hf_2O, and (e) $P\bar{4}m2$-Hf_2O_3.

where H_v, G, and B are the hardness (GPa), shear modulus (GPa), and bulk modulus (GPa), respectively. The parameter k is the Pugh's modulus ratio, namely, $k = G/B$.

Anisotropic elasticity of single crystals has a great effect on the elastic behavior of polycrystals and can exert its influence on the anisotropic plastic deformation and crack behavior. Most materials are elastically anisotropic, and their Young's modulus will be an anisotropic property. It is useful in practice to show the directional variation of Young's modulus by three-dimensional diagrams, where deviations from sphericity directly reflect the degree and direction of anisotropy. We calculated the elastic anisotropy of five special phases: $P\bar{6}2m$-HfO, $Pnnm$-Hf_2O, $Imm2$-Hf_5O_2, $P\bar{3}1m$-Hf_2O, and $P\bar{4}m2$-Hf_2O_3. As shown in Fig. 10, it is readily evident that $P\bar{6}2m$-HfO, $Imm2$-Hf_5O_2, $P\bar{3}1m$-Hf_2O, and $P\bar{4}m2$-Hf_2O_3 exhibit a moderate amount of anisotropy of Young's modulus, particularly $Imm2$-Hf_5O_2, $P\bar{3}1m$-Hf_2O while $Pnnm$-Hf_2O tends to be considerably less anisotropic. The directional dependence of the Young's modulus for hexagonal, orthorhombic, trigonal, and tetragonal crystals can be calculated according to the elastic compliance constants [34] (see the Supplemental Material [28] for detail).

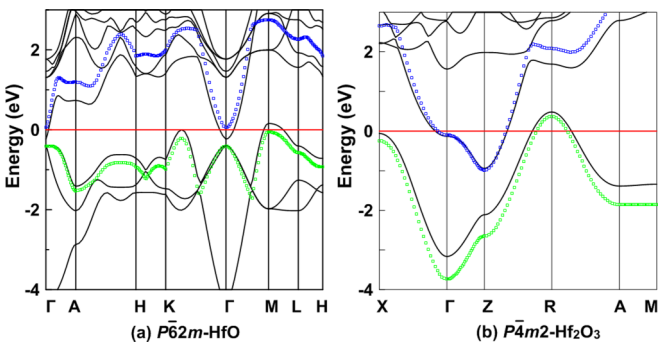

FIG. 11. (Color online) Band structures of $P\bar{6}2m$-HfO and $P\bar{4}m2$-Hf_2O_3 at 0 GPa. The Fermi energy is set to zero. Hybrid functional is believed to give the same level of accuracy as more rigorous GW quasiparticle calculations. The black lines represent the band structure calculated by DFT-GGA method and open-circle lines denote the band structure calculated by hybrid functional HSE06 method.

D. Electronic structure of Hf-O compounds

Band structures of Hf-O compounds at 0 GPa (including phases stable at both zero and high pressure) are listed in Supplemental Material Fig. S3 [28]. Band structures of $P\bar{6}2m$-HfO and $P\bar{4}m2$-Hf_2O_3 at 0 GPa are depicted in Fig. 11. $P\bar{4}m2$-Hf_2O_3 shows the semimetallic character based on both DFT band structure and hybrid functional HSE06 band structure. Interestingly, the chemical behavior of Zr and Hf are similar, $P\bar{6}2m$-ZrO has been confirmed to be a semimetal according to the band structures from both DFT and HSE06 calculations [30], therefore the band structure of $P\bar{6}2m$-HfO calculated by HSE06 is supposed to be similar. However in the more accurate approach for the HSE06 result it turns out that $P\bar{6}2m$-HfO has the tiny band gap 0.112 eV between the conduction band and valence band while the DFT-GGA band structure shows that very few states at the Fermi level and $P\bar{6}2m$-HfO should be a semimetal. Given that HSE06 is more accurate than the DFT method, we therefore treat $P\bar{6}2m$-HfO as a semiconductor instead of a semimetal according to its calculated HSE06 band structure.

Total and partial densities of states (DOS) calculated by DFT are presented in Fig. 13. $R\bar{3}$-Hf_6O, $R\bar{3}c$-Hf_3O, $Imm2$-Hf_5O_2, $R\bar{3}$-$Hf_{12}O_5$, $P\bar{3}1m$-Hf_2O, $Pnnm$-Hf_2O, $I4_1/amd$-Hf_2O, and $C2/m$-Hf_3O_2 are predicted to be metallic with a sizable density of states at the Fermi level and the interactions between

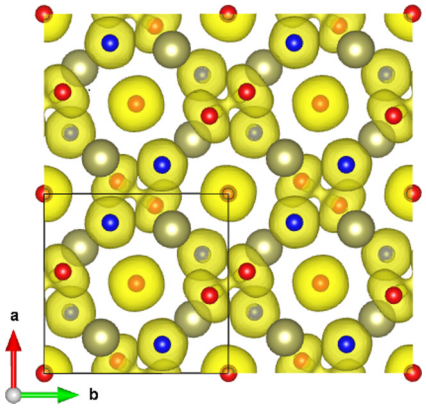

FIG. 12. (Color online) ELF isosurface (ELF = 0.62) for HfO_3. Blue and red atoms represent oxide O^{2-} and peroxide $[O\text{-}O]^{2-}$ ions, respectively.

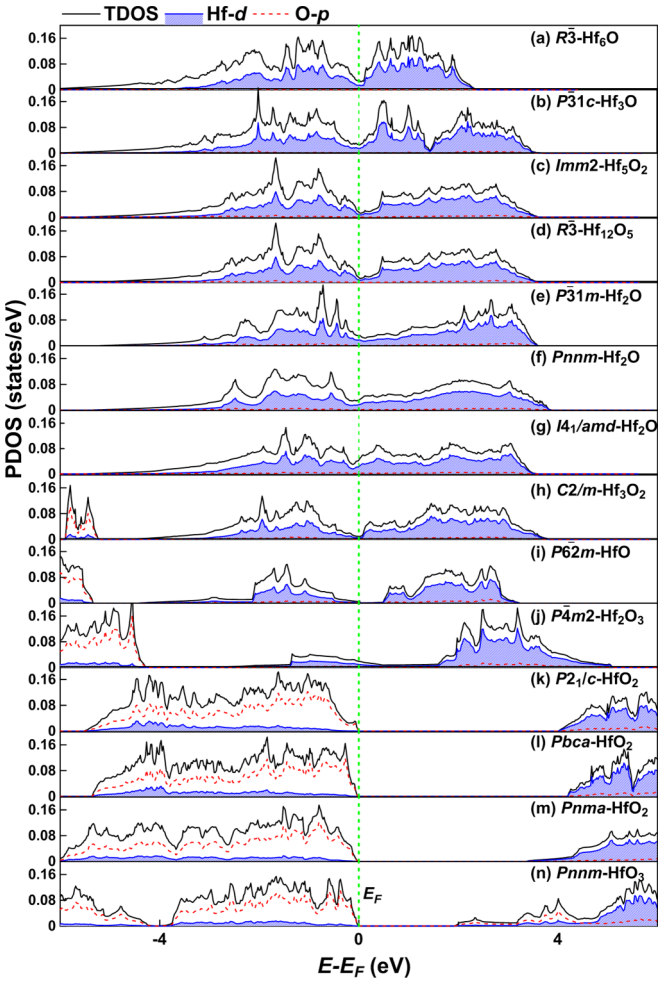

FIG. 13. (Color online) The normalized (per electron) total (TDOS) and partial densities of states (PDOS) of hafnium oxides at 0 GPa. The Fermi energy is set to zero.

the Hf-*d* orbitals are responsible for their metallicity. The DFT band gaps of $P2_1/c$-HfO_2, *Pbca*-HfO_2, *Pnma*-HfO_2, and *Pnnm*-HfO_3 are 4.01, 4.18, 3.36, and 1.92 eV, respectively, and the highest occupied states are all derived mainly from O-*p* orbitals, as shown in Figs. 13(j)–13(m). Therefore, according to their electronic character, Hf-O compounds can be divided into three types: metallic, including $R\bar{3}$-Hf_6O, $R\bar{3}c$-Hf_3O, *Imm*2- Hf_5O_2, $R\bar{3}$- $Hf_{12}O_5$, $P\bar{3}1m$-Hf_2O, *Pnnm*-Hf_2O, $I4_1/amd$-Hf_2O, and $C2/m$-Hf_3O_2; semimetallic, including $P\bar{4}m2$-Hf_2O_3; insulating or semiconducting, including $P\bar{6}2m$-HfO, $P2_1/c$-HfO_2, *Pbca*-HfO_2, *Pnma*-HfO_2, and *Pnnm*-HfO_3. The electron localization function (ELF) clearly reveals a special feature of HfO_3: the coexistence of oxide O^{2-} and peroxide $[O\text{-}O]^{2-}$ anions (Fig. 12). The peroxide is responsible for gap states, which significantly reduce the electronic band gap of HfO_2 [Fig. 13(m)]. To obtain further insight, we applied the atoms in molecules (AIM) theory developed by Bader [42]. Bader charges are +2.5 for Hf, −0.68 for peroxide anion, and −1.16 for oxide anion in HfO_3 at 110 GPa, which shows a significantly ionic character of bonding. Valence electrons localize on O atoms in other Hf-O compounds (see ELF plots for other Hf-O compounds in Supplemental Material Fig. S4 [28]).

IV. CONCLUSIONS

We have systematically predicted stable compounds and crystal structures in the Hf-O system at pressures up to 120 GPa using the *ab initio* evolutionary algorithm USPEX. Several new stable compounds, including *Imm*2-Hf_5O_2, $C2/m$-Hf_3O_2, $P\bar{6}2m$-HfO, and *Pnnm*-HfO_3 are found for the first time. *Pnnm*-Hf_2O and $I4_1/amd$-Hf_2O, which are the new high-pressure phases of Hf_2O, are also discovered. HfO_3 shows an interesting structure, simultaneously containing oxide O^{2-} and peroxide $[O\text{-}O]^{2-}$ anions. Our results demonstrate that Hf_3O_2 is more ductile than other Hf-O compounds, and the hardest compound is HfO instead of OII-HfO_2. The superior mechanical properties of $P\bar{6}2m$-HfO, such as bulk modulus *B*, shear modulus *G*, Young's modulus *E*, and hardness H_v, can be attributed to the peculiar combination of strong Hf-O and Hf-Hf bonds. *Pnnm*-Hf_2O, *Imm*2-Hf_5O_2, $P\bar{3}1m$-Hf_2O, and $P\bar{4}m2$-Hf_2O_3 also show excellent mechanical properties. Clearly, high O content is not a key factor affecting the mechanical properties of Hf-O compounds. Suboxides Hf_6O, Hf_3O, $Hf_{12}O_5$, and $P\bar{3}1m$-Hf_2O based on hcp-Hf sublattice provide easy pathways for absorbing or desorbing oxygen. The recognition of the common structural features between $P\bar{6}2m$-HfO and *ω*-Hf gives further insight into the physical properties and suggests that HfO can be made as a hard semimetallic coating on *ω*-Hf substrate. *Pnnm*-Hf_2O, *Imm*2-Hf_5O_2, $P\bar{3}1m$-Hf_2O, and $P\bar{4}m2$-Hf_2O_3 phases in particular can be quenched to ambient pressure and can be candidates for applications requiring mechanically strong materials.

ACKNOWLEDGMENTS

This work was supported by the National Science Foundation (Grant No. EAR-1114313), DARPA (Grant No. W31P4Q1210008), the Basic Research Foundation of NWPU (Grant No. JCY20130114), the Natural Science Foundation of China (Grants No. 51372203 and No. 51332004), the Foreign Talents Introduction, the Academic Exchange Program of China (Grant No. B08040), and the Government (Grant No. 14.A12.31.0003) of the Russian Federation. The computational resources at the High Performance Computing Center of NWPU are also gratefully acknowledged. Z.W. thanks the support from China Scholarship Council (No. 201408320093) and the Natural Science Foundation of Jiangsu Province (Grant No. BK20130859).

[1] J. Choi, Y. Mao, and J. Chang, Mater. Sci. Eng., R **72**, 97 (2011).
[2] K.-L. Lin, T.-H. Hou, J. Shieh, J.-H. Lin, C.-T. Chou, and Y.-J. Lee, J. Appl. Phys. **109**, 084104 (2011).
[3] Y. Al-Khatatbeh, K. K. M. Lee, and B. Kiefer, Phys. Rev. B **82**, 144106 (2010).
[4] Y.-W. Chung and W. D. Sproul, MRS Bull. **28**, 164 (2003).

[5] J. E. Lowther, MRS Bull. **28**, 189 (2003).
[6] H. Xia, G. Parthasarathy, H. Luo, Y. K. Vohra, and A. L. Ruoff, Phys. Rev. B **42**, 6736 (1990).
[7] R. Ahuja, J. M. Wills, B. Johansson, and O. Eriksson, Phys. Rev. B **48**, 16269 (1993).
[8] T. Tsuji, J. Nucl. Mater. **247**, 63 (1997).
[9] T. B. Massalski, H. Okamoto, P. R. Subramanian, L. Kacprzak, and W. W. Scott, *Binary Alloy Phase Diagrams* (American Society for Metals Metals Park, OH, 1986) Vol. 1.
[10] M. Hirabayashi, S. Yamaguchi, and T. Arai, J. Phys. Soc. Jpn. **35**, 473 (1973).
[11] M. Hirabayashi, S. Yamaguchi, T. Arai, H. Asano, and S. Hashimoto, J. Phys. Soc. Jpn. **32**, 1157 (1972).
[12] A. V. Ruban, V. I. Baykov, B. Johansson, V. V. Dmitriev, and M. S. Blanter, Phys. Rev. B **82**, 134110 (2010).
[13] B. Paul Burton, A. van de Walle, and H. T. Stokes, J. Phys. Soc. Jpn. **81**, 014004 (2012).
[14] K.-H. Xue, P. Blaise, L. R. C. Fonseca, and Y. Nishi, Phys. Rev. Lett. **110**, 065502 (2013).
[15] S. Desgreniers and K. Lagarec, Phys. Rev. B **59**, 8467 (1999).
[16] J. Tang, M. Kai, Y. Kobayashi, S. Endo, O. Shimomura, T. Kikegawa, and T. Ashida, Prop. Earth Planet. Sci. Mater. High Press. Temp. 401 (1998).
[17] J. Kang, E.-C. Lee, and K. J. Chang, Phys. Rev. B **68**, 054106 (2003).
[18] D. M. Adams, S. Leonard, D. R. Russell, and R. J. Cernik, J. Phys. Chem. Solids **52**, 1181 (1991).
[19] O. Ohtaka, H. Fukui, T. Kunisada, T. Fujisawa, K. Funakoshi, W. Utsumi, T. Irifune, K. Kuroda, and T. Kikegawa, J. Am. Ceram. Soc. **84**, 1369 (2001).
[20] X.-Q. Chen, H. Niu, D. Li, and Y. Li, Intermetallics **19**, 1275 (2011).
[21] A. R. Oganov and C. W. Glass, J. Chem. Phys. **124**, 244704 (2006).
[22] A. O. Lyakhov, A. R. Oganov, H. T. Stokes, and Q. Zhu, Comput. Phys. Commun. **184**, 1172 (2013).
[23] A. R. Oganov, A. O. Lyakhov, and M. Valle, Acc. Chem. Res. **44**, 227 (2011).
[24] J. P. Perdew, K. Burke, and M. Ernzerhof, Phys. Rev. Lett. **77**, 3865 (1996).
[25] G. Kresse and J. Furthmüller, Phys. Rev. B **54**, 11169 (1996).
[26] P. E. Blöchl, Phys. Rev. B **50**, 17953 (1994).
[27] A. Togo, F. Oba, and I. Tanaka, Phys. Rev. B **78**, 134106 (2008).
[28] See Supplemental Material at http://link.aps.org/supplemental/10.1103/PhysRevB.92.184104 for the detailed convex hull information of Hf-O compounds at a certain pressure in Fig. S1 and the calculated phonon dispersion curves for Hf-O compounds are in Fig. S2. Band structures of all the Hf-O compounds at 0 GPa are shown in Fig. S3. Apart from Pnnm-HfO3, the ELF plots for other Hf-O compounds are also provided in Fig. S4. The equations for calculating bulk modulus and shear modulus from the Reuss and Voigt are listed in Eq. S1-4. The equations for calculating the directional dependence of the Young's modulus for hexagonal, orthorhombic, trigonal, and tetragonal crystals according to the elastic compliance constants are listed in Eq. S5-8 . Equation S9-13 give the criteria of mechanical stability for orthorhombic, tetragonal, trigonal and hexagonal crystal.
[29] B. P. Burton and A. van de Walle, Calphad **37**, 151 (2012).
[30] J. Zhang, A. R. Oganov, X. Li, H. Dong, and Q. Zeng, Phys. Chem. Chem. Phys., **17**, 17301 (2015).
[31] F. Birch, J. Geophys. Res. **57**, 227 (1952).
[32] R. Jeanloz, Phys. Rev. B **38**, 805 (1988).
[33] F. Birch, J. Geophys. Res. **83**, 1257 (1978).
[34] J. F. Nye, *Physical Properties of Crystals: Their Representation by Tensors and Matrices* (Clarendon Press, Oxford, 1985).
[35] A. F. Wells, *Structural Inorganic Chemistry* (Oxford University Press, New York, 1986).
[36] Y. Liu, A. R. Oganov, S. Wang, Q. Zhu, X. Dong, and G. Kresse, Sci. Rep. **5** (2015).
[37] J. Haines, J. M. Léger, S. Hull, J. P. Petitet, A. S. Pereira, C. A. Perottoni, and J. A. H. da Jornada, J. Am. Ceram. Soc. **80**, 1910 (1997).
[38] A. Reuss, Z. Angew. Math. Mech. **9**, 49 (1929).
[39] W. Voigt, *Lehrbuch der Kristallphysik* (B.G. Teubner, Leipzig, 1910), Vol. 34, pp. 830–831.
[40] R. Hill, Proc. Phys. Soc., London, Sect. A **65**, 349 (1952).
[41] M. Okutomi, M. Kasamatsu, K. Tsukamoto, S. Shiratori, and F. Uchiyama, Appl. Phys. Lett. **44**, 1132 (1984).
[42] R. F. W. Bader, *Atoms in Molecules: A Quantum Theory* (Oxford University Press, Oxford, 1990).